Modified HSE06 functional applied to anatase TiO_2: influence of exchange fraction on the quasiparticle electronic structure and optical response

Sruthil Lal, S. B.; Devaraj, M.; Posselt, M.; Aravindh Sd, A.; Sharan, A.;

Originally published:

October 2022

Electronic Structure 4(2022), 045001

DOI: https://doi.org/10.1088/2516-1075/ac8f03

Modified HSE06 functional applied to anatase TiO_2 : influence of exchange fraction on the quasiparticle electronic structure and optical response

To cite this article before publication: Sruthil lal S B *et al* 2022 *Electron. Struct.* in press https://doi.org/10.1088/2516-1075/ac8f03

Modified HSE06 functional applied to anatase TiO_2: influence of exchange fraction on the quasiparticle electronic structure and optical response

Sruthil Lal S.B

Department of Physics, Pondicherry University, Kalapet, Puducherry, India

E-mail: getsruthil@gmail.com

D Murali

Indian Institute of Information Technology Design and Manufacturing (IIITDM), Kurnool, Andhra Pradesh, India

Matthias Posselt

Helmholtz-Zentrum Dresden-Rossendorf, Bautzner Landstraße 400, 01328 Dresden, Germany

Assa Aravindh Sasikala Devi

Nano and molecular systems research unit, P.O.Box 8000, FI-90014, University of Oulu, Oulu, Finland

Alok Sharan

Department of Physics, Pondicherry University, Kalapet, Puducherry, India

E-mail: alok.phy@pondiuni.edu.in

Abstract. The influence of non-interacting Kohn-Sham Hamiltonian on the non-self consistent $GW(G_0W_0)$ quasiparticle gap and Bethe-Salpeter-Equation(BSE) optical spectra of anatase TiO_2 is systematically evaluated. G_0W_0 and BSE calculations are carried out starting with HSE06 (Heyd-Scuseria-Ernzerhof) type functionals containing 20, 25 and 30 % exact Hartree-Fock exchange. The results are also compared against G_0W_0+BSE calculations starting from semi-local(PBE) functionals. Our results indicate that the G_0W_0 and BSE calculations of anatase TiO_2 depend critically on the mean-field starting point, wherein its dependence is mainly introduced through the dielectric screening evaluated at the intermediate G_0W_0. We find that the band dispersion, density of states, and consequently the oscillator strengths of optical excitation and spatial localization of excitons are insensitive to the starting points while the quasiparticle gap, optical gap and exciton binding energies are strongly affected. G_0W_0 quasiparticle gap of anatase TiO_2 computed over hybrid functional starting points is typically overestimated compared to measured values. However, by varying the amount of exact exchange, the dielectric screening can be tuned, and thus the quasiparticle gap. Exciton binding energy is shown to increase in proportion to the increase of the amount of exact exchange. A simple extrapolation of the calculated data leads to the exact match with the recently measured value with 13 % of the exact exchange. Systematic analysis of G_0W_0+BSE calculation starting from screened hybrid functionals provided in this study forms a reference for all such future calculations of pristine anatase TiO_2 and its derivatives.

1. Introduction

Titanium Dioxide (TiO_2) is one of the most widely explored metal-oxides owing to its charge transport and oxidation properties, abundance, non-toxicity, and corrosion resistance. TiO_2 finds promising applications in photocatalysis[1–3], opto-electronic devices[4, 5], dye-sensitized solar cells(DSSC)[4, 6–9], treatment of pollutants[10, 11], production of hydrocarbon fuels[12, 13], antimicrobial coatings[14], nonlinear optical applications[15] and so on. Among the naturally occurring TiO_2 polymorphs, the anatase form is found to be photocatalytically most active phase than rutile and brookite[16–20]. Anatase has a wider optical gap and smaller electron effective mass, which leads to its higher electron mobility[6, 21–23]. It plays a key role in the injection process of solar cells yielding high conversion efficiency[4–7, 24]. Tuning of electronic and optical properties of anatase TiO_2 for tailor-made applications has been an active area of research[25], exploring various strategies like doping with noble gas[26], various metals[27–35] as well as by strain engineering[36, 37].

Processing materials for tailor-made applications requires a fundamental understanding of their electronic and optical excitations. The excited carriers and the associated perturbation in a material have a many-body character and operate collectively as quasiparticles. Experimentally, the quasiparticle character of electronic excitation is captured in photoemission(PES) and inverse photoemission spectroscopy(IPES). Due to the quasiparticle nature of the excitation, the energies measured using (I)PES are called quasiparticle energies. Similarly, optical excitation creates electrons and holes, paired into bound states due to the strong Coulomb interaction forming quasiparticles called excitons.

For quantitative modeling of photoemission and optical absorption of pristine anatase TiO_2, it is necessary to invoke many-body effects[28, 38–44]. One must include the many-body effects in the electronic and optical spectra by employing the many-body perturbation theory(MBPT). In MBPT, the photoemission spectrum is modeled via the GW approximation (GWA)[45–47]. On top of GW calculation, the Bethe-Salpeter equation (BSE)[48] is solved to include electron-hole interaction during optical absorption.

The standard GW calculation starts with a Kohn-Sham (KS) DFT calculation to obtain a non-interacting (single-particle) ground state. The GWA is then applied perturbatively to the KS orbitals $|\phi_i^{KS}\rangle$ and one-electron energies ϵ_i^{KS}. This results in different GW flavors depending on whether $|\phi_i^{KS}\rangle$ and/or ϵ_i^{KS} determined self-consistently or not. Self-consistent GW calculations starting from semi-local(PBE) functional overestimate the quasiparticle gap of TiO_2, worsening the agreement with experiments[49]. Therefore, the non-self consistent GW calculation (G_0W_0) is used for all practical calculation of TiO_2[50–55]. However, due to the lack of self-consistency, G_0W_0 calculations become sensitive to the initial non-interacting KS-DFT Hamiltonian(H_0).

The starting point sensitivity of the G_0W_0 method is usually addressed by choosing an H_0 such that the resulting quasiparticle correction is minimized, hence justifying the use of GWA as perturbation[46, 56–58]. For G_0W_0 and BSE calculations of pristine anatase TiO_2, semi-local(PBE) DFT wave functions were explored as the starting points[39–42, 49, 59, 60]. G_0W_0 quasiparticle gaps obtained from such calculations show huge variability. For oxides and materials with d-orbitals close to the band edges, hybrid functional[61–64] provides a more reasonable and physically accurate initial KS DFT wave function compared to local/semi-local functionals[65–71]. In this direction, we assess the performance of hybrid functional as the starting point for G_0W_0 and BSE of anatase TiO_2 in the present work. To the best of our knowledge, apart from a recent study in Ref. [72], G_0W_0+BSE calculations of pristine anatase TiO_2 exploring the role of hybrid functional as starting points are not available.

Hybrid functional have certain inherent advantages compared to semi-local functional[73–75] as the starting point for G_0W_0 calculations. Hybrid functional remedies the bandgap underestimation[73–80] caused by local/semi-local functional. Formally, hybrid functionals describe non-local two-particle scattering processes[81, 82]; therefore, the resulting wave functions are close to the quasiparticle wave functions. Hybrid functional provides the correct ordering and occupation of bands and the localization of orbitals leading to accurate quasiparticle properties and dielectric functions[65, 69, 70, 72, 83, 84]. Besides hybrid functional, the DFT+U method is commonly used to represent localization of orbitals. However, DFT+U introduces unreasonable lattice distortions when suboptimal U values are used[85–87]. Moreover, unlike DFT+U, hybrid functional treat delocalized and localized states on the same footing through the orbital dependence of the Hartree-Fock(HF) exchange. Hence, for TiO_2 and other $3d$ transition-metal compounds, orbital-dependent screening present in the hybrid functional is the most effective way to address the starting point dependence of G_0W_0 associated with localized d orbitals[88].

In this study, hybrid functional[63, 89, 90] DFT wavefunctions are used as the starting point for G_0W_0 and subsequent BSE calculations of anatase TiO_2. HSE06-like screened hybrid functional as parametrized by Heyd-Scuseria-Ernzerhof[63, 89, 90] are employed for the calculations. The amount of exact exchange (α) contained in the existing formulations of hybrid functional is not a universal entity. Rather, α is a material-dependent parameter. For a given system, one could choose an optimal α so that the subsequent G_0W_0+BSE calculation gives an accurate value for quasiparticle gap and optical gap. The rationale for varying α is its relation to the dielectric screening of the material[91–96]. In the case of uncorrelated d electronic systems like TiO_2, α is proportional to $1/\epsilon_\infty$, where ϵ_∞ is the dielectric constant of the material in the limit of very large frequencies[55, 95, 97, 98]. In the present work, the value of α contained HSE06-like functional(HSE06(α)) is varied, and its effects on the DFT electronic structure of anatase TiO_2 is investigated. The role of α on the G_0W_0 quasiparticle gap, BSE optical spectra and exciton binding energy is also investigated starting from HSE06(α) wavefunctions.

The article is organized as follows: Computational schemes for DFT and MBPT calculations are summarized in Sec. 2. Sec. 3 compares the ground state DFT electronic structure using PBE and HSE06 type functional. Further, the variation of G_0W_0 quasiparticle gaps and BSE spectra of anatase TiO_2 calculated on top of PBE and HSE06 type starting wave functions are discussed. The role of exchange-correlation, and in particular, the effect of the amount of exact exchange present in HSE06 type functional on the DFT and MBPT calculations of anatase TiO_2 are discussed in detail. We conclude the article in Sec. 4 with a discussion of our results, scope and limitations.

2. Computational details

2.1. Semi-local and hybrid DFT

All ground state DFT, GW, and BSE calculations are performed using the Vienna ab-initio simulation package (VASP) [99–103]. Recommended projector augmented wave(PAW) potentials[104, 105] supplied with VASP were employed for all atoms to describe the core-valence interactions. These PAW potentials are optimized for GW, as opposed to the standard PAW potentials, and provide an accurate description of scattering properties even at higher energies[103]. Besides the Ti $4s$ & $3d$ and O $2s$ & $2p$ valence states, the shallow Ti $3s$ & $3p$ core states are also treated as valence electrons. Their inclusion is essential for an accurate calculation of quasiparticle energy gaps[40], the omission of which causes the quasiparticle bandgap to vary by about 0.3 eV[49]. Gaussian smearing with $\sigma = 0.05$ eV was used to broaden the one electron levels. Based on the convergence of total free energy, we have set 520 eV as kinetic energy cut-off to describe the plane waves included in the basis set. An unshifted Γ-centered $6 \times 6 \times 3$ Monkhorst-Pack grid [106] is used for sampling the body-centered tetragonal Brillouin zone of anatase TiO_2. Initially, the geometry of the conventional unit cell of bulk anatase TiO_2 is relaxed using the GGA (PBE) functional with force and energy convergence thresholds of 10^{-5} eV/Å and 10^{-6} eV, respectively. The relaxed tetragonal lattice is characterized by lattice constants: $a = 3.805$ Å and $c = 9.781$ Å, which are in reasonable agreement with lattice parameters measured in experiments[107–109].

The electronic structure of anatase TiO_2 is then calculated by introducing the HSE06[61–63] functional. In the present investigation, we maintain the screening parameter defining HSE06 type functional at $\omega = 0.20$ Å^{-1} (corresponding to a screening length $r_s = 2/\omega = 10$ Å). However, in the spirit of Ref. [55, 110–115] amount of exact exchange(α) is varied to understand its effect on the spectral properties of pristine anatase TiO_2. We focus our attention on three values for exchange fractions; 20%, 25%

(standard HSE06) and 30% for which DFT electronic structure is computed, and the variation of the many-body response resulting from them are evaluated at G_0W_0+BSE level. DFT calculation with a given α in the description of HSE06 type functional is henceforth labelled as HSE06(α).

2.2. G_0W_0 and BSE calculations

The many-body electron-electron interaction in the GWA is represented by the electronic self-energy, which is approximated as $\Sigma = iGW$, where G is the one-particle Green's function, and W is the dynamically screened Coulomb interaction[57, 116, 117]. The Green's function can be expressed by using the electronic eigenvalues and wave functions computed for the DFT Kohn-Sham system. The screened-Coulomb interaction(W) is obtained from the polarizability, which is given by the product of the non-interacting electron and hole Greens's functions[118, 119]. In the non-self-consistent GW (G_0W_0) calculations, GWA uses non-interacting Kohn-Sham (KS) orbitals $|\phi_i^{KS}\rangle$ as starting point. The self-energy Σ is then approximated as $\Sigma = iG^{KS}W^{KS}$. Here, G^{KS} is the Kohn-Sham one-particle Green's function and W^{KS} is the screened Coulomb interaction constructed from G^{KS} using the random-phase approximation. In the present work, the orbitals $|\phi_i^{KS}\rangle$ of well-converged ground state DFT calculation with HSE06(α) functional is used as the starting point for G_0W_0 calculations. In the perturbative regime, the difference between the GW self-energy Σ^{GW} and Kohn-Sham exchange-correlation potential v_{xc}, is to be regarded as small with respect to the entire Hamiltonian. The first-order correction $\epsilon_i^{G_0W_0}$ to the input KS energies ϵ_i^{KS} is obtained by solving the quasiparticle equation

$$\epsilon_i^{G_0W_0} - \epsilon_i^{KS} = Z_i \langle\phi_i^{KS}|\, \Sigma^{G_0W_0}(\epsilon_i^{G_0W_0}) - v_{xc}[\rho]\, |\phi_i^{KS}\rangle \tag{1}$$

where $\epsilon_i^{G_0W_0}$ represents the quasiparticle energy, Z_i is the normalization factor for the orbital and the index i runs over states and k points in a solid.

The Bethe-Salpeter equation for two particle-Green's functions is solved to calculate the optical properties[119–121]. In the coupled electron-hole basis, the BSE turns into an eigenvalue problem;

$$(E_c - E_v)\, A_{vc}^S + \sum_{v'c'} K_{vc,v'c'}(\Omega_S) A_{v'c'}^S = \Omega_S A_{vc}^S \tag{2}$$

where $c(v)$ denotes the conduction (valence) band, and E_c and E_v, respectively, are the energies of electron in the conduction band and hole in the valance band. K_{e-h} represents the electron-hole interaction kernel. Ω_S is the exciton energy and A_{vc}^S is the eigenvector of the BSE. The first term on the left side of Eq. 2 describes the uncorrelated electron-hole pair, while the second term accounts for the interaction between bound electron and hole. This form is referred to as the Tamm-Dancoff approximation to BSE[122–124] and corresponding VASP implementation is used in the present work[51, 103, 125]. From the solution of the BSE, the dielectric function and oscillator strengths of optical transitions of anatase TiO_2 are computed for parallel and perpendicular(with respect to the crystallographic c axis) polarizations. Further, the excitation mechanism is explained by examining the exciton amplitude projections on the quasiparticle bandstructure in fatband form[126–129]. Based on the analysis, the nature of photo-generated charge carriers, their origin and spatial localization in the anatase TiO_2 are also presented. The influence of amount of exact exchange ((PBE), 20, 25 and 30%) on the optical gap, binding energy and spatial localization of excitons are further addressed.

3. Results and Discussion

3.1. DFT bandstructure with PBE and HSE06(α) functionals

To understand how the exact exchange contribution(α) affects the bandgap, DFT calculations were first carried out with HSE06 type functional by varying α from 15% to 35% with an interval of 5%. This range of α for hybrid functionals yields excellent results for a large class of systems[94, 96, 115, 130]. Fig.1 shows that for several k-point grids, the difference between the corresponding bandgap is below 0.05 eV, so a good convergence is reached in this range of α. For a representative case of $6 \times 6 \times 3$ k-grid sampling, the HSE06(α) band gap increases from 3.04 eV to 4.36 eV as the fraction of exchange is increased from 15% to 35%. This apparent increase in hybrid DFT gap in linear proportion to the increase in α (≈ 0.33 eV for every 5% increase in α) is consistent with the trend observed for hybrid functionals elsewhere[96, 111, 114, 115].

To assess the influence of exchange-correlation on the bandstructure, the PBE and HSE06(α) bandstructure of TiO_2 is compared. The general features of the electronic structure of anatase TiO_2 using HSE06(α) are discussed by taking HSE06(20) as a representative case. The PBE and HSE06(20) bandstructure of anatase TiO_2 along the high symmetric directions in the irreducible Brillouin zone is shown in Fig.2. Interestingly, the dispersion of conduction and valence bands near the respective band edges remain similar with both GGA and HSE06(α) functionals. The addition of exact exchange shifts the HSE06(α) conduction bands to higher energies with respect to the PBE counterparts, almost uniformly across all the bands and k-points. Nevertheless, the valence bands remain unaffected irrespective of PBE and HSE06(α) exchange-correlation functionals. The amount of shift is proportional to the value of α. With $\alpha = 20$ %, HSE06(20) conduction bands move up by 1.23 eV with respect to PBE conduction bands; hence, the overall band gap opens up to 3.34 eV. The bandgap is indirect with CBM at Γ point and VBM at $0.91\Gamma \rightarrow M$[115, 131], consistent with the literature [39, 41, 132].

HSE06(20) density of states of anatase TiO_2 shown in Fig.3 reveals that O-2p orbitals occupy the top of the valence band. Conduction bands populated primarily by the Ti-3d like orbitals are split into two groups, one lying above and one below 4.5 eV. The band splitting occurs as a result of TiO_6 octahedral coordination in TiO_2 and associated crystal field splitting of Ti-3d orbitals into triply degenerate t_{2g} (states below 4.5 eV) and doubly degenerate e_g (states above 4.5 eV) states[41, 133–135]. The joint contribution of Ti-3d and O-2p orbitals near the band edges, coupled with strong dispersion of bands indicates the hybridization of O-2p and Ti-3d orbitals. Hybridization of orbitals in the vicinity of the Fermi level leads to the formation of covalent Ti-O bonds[38, 133, 136, 137]. The bond's covalent nature has also been established by determining the charge enclosed within the Bader charge volume[138] of respective ions. From the Bader charge analysis, we arrive at Bader charge-based ionic states of $Ti^{2.26+}$ and $O^{1.12-}$. The departure of ionic charge states from the expected nominal ionic valences of +4 and -2 for Ti and O, respectively, indicates the strong covalent character of the Ti-O bond. With HSE06(α = 25, 30%) and PBE functionals, the situation regarding the band dispersion and density of states are very similar except for the variation in the bandgap(supplementary information).

KS band gaps obtained using HSE06(α) functional in the present work are consistent with previous reports. We calculate a bandgap of 3.68 eV with standard HSE06(with α = 0.25). We can compare this with the following reported values calculated using the standard hybrid functionals; which are 3.60 [41, 139], 3.57[140], 3.58[141], 3.59[95], 3.60[142], and 3.89 eV[143]. Ref. [144] reports a gap of 3.38 eV with standard HSE06 functional[144]. Similar to our work, Ref. [130] varied the mixing fraction of hybrid(HSE) functional and found an indirect bandgap of 3.20 eV with 22% exact exchange. 20% exchange fraction in the screened HSE06 functional tested for anatase TiO_2 in Ref [145] obtained a bandgap of 3.05 eV[145]. The considerable variability of hybrid DFT bandgaps of TiO_2 is evident across the literature, and it owes partly to minor differences in initial structure and computational setup.

We observe that the bonding character, band dispersion and density of states are very similar irrespective of whether the exchange-correlation present in the non-interacting KS Hamiltonian is either semi-local(PBE) or non-local(hybrid functionals). However, the bandgap of the materials is strongly affected by the addition of non-local HF exchange. Due to its proportionality to the dielectric screening of the material, increasing the exchange fraction (α) increases the bandgap in linear proportion to α. Being an uncorrelated metal oxide, it is fair to assume that the linear relation of TiO_2 bandgap to α is valid. Relying on the validity of this relation, in the discussion that follows, we restrict our G_0W_0 and BSE calculations only on PBE, and HSE06(20, 25, 30 %) DFT eigensystems. For all other G_0W_0 and BSE calculations, the k-point grid has been fixed to a $6 \times 6 \times 3$ grid. Typically, this k-point sampling density is more than sufficient to accurately represent the screened exchange interaction in metals and semiconductors, whereas dealing with bare exchange requires at least a $(12 \times 12 \times 12)$ grid[90]. This demonstrates the computational efficiency one can achieve when screened hybrid exchange functionals are being used.

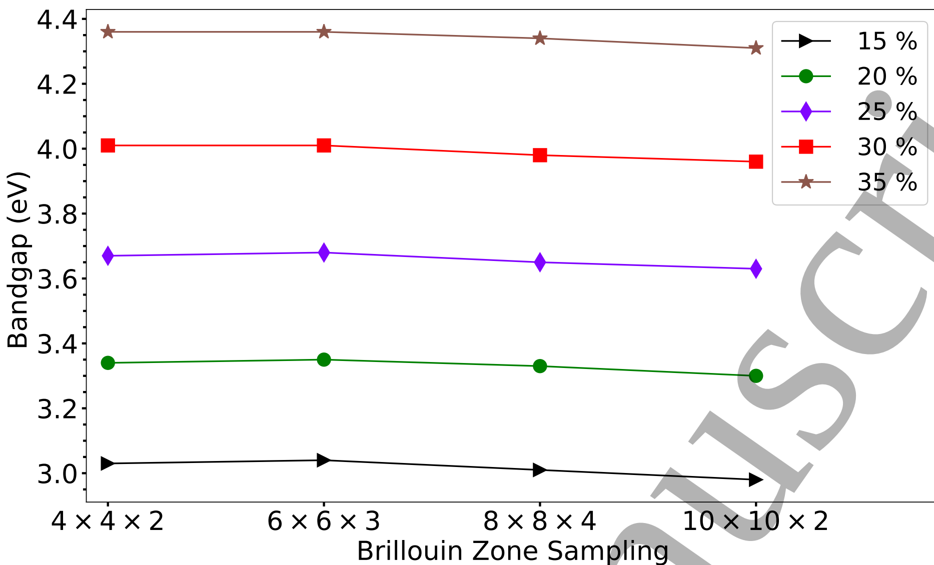

Figure 1. The convergence of HSE06(α) bandgap for various values of exchange fraction (α = 15, 20, 25, 30 and 35%) with respect to Brillouin zone sampling size. For $6 \times 6 \times 3$ k-point grid, as α increases band gap also increases at an approximate rate of 0.66 eV per 10% increase in the α, which is represented quantitatively by a straight line $E_g(eV) = 0.066\alpha(\%) + 2.038$. The bandgap extrapolated to $\alpha = 0$ closely matches the PBE bandgap (2.11 eV).

3.2. G_0W_0 *Quasiparticle corrections*

We have determined G_0W_0 quasiparticle corrections on top of DFT eigenvalues obtained with PBE and HSE06(α) functionals. In the remainder of the text, the former is labelled as G_0W_0@PBE and the latter G_0W_0@HSE06(α). The convergence of the G_0W_0 bandgap is carefully examined for the number of empty states(virtual orbitals) and frequency points in the real space for the response functions. For all G_0W_0 calculations, we have set a rather conservative cut-off of 150 eV for the basis set for the G_0W_0 response function. The details of the convergence study are summarized in Fig.4 for representative cases of G_0W_0@PBE and G_0W_0@HSE06(20). Within the range of values of convergence parameters used in this work, quasiparticle gaps and HOMO and LUMO energies show similar convergence rates irrespective of the PBE or HSE06(α) starting wave functions. To calculate the frequency-dependent dielectric matrix, 256 bands(48 occupied and 208 virtual orbitals), 100 points on the frequency grid, and a $6 \times 6 \times 3$ gamma-centered k-point were used. With this set-up, the quasiparticle bandgap is converged to within 0.01 eV. For even better convergence, one has to use a larger energy cut-off, denser k-point sampling and more empty states, which would make the calculation practically impossible due to forbidding memory requirements[146].

Table 1 presents the calculated G_0W_0 bandgaps on PBE and HSE06(α) starting points compared to the literature data. Our results show that the exchange-correlation functional chosen while constructing the initial wave functions significantly affect the quasiparticle gap of anatase TiO_2. G_0W_0 quasiparticle gap calculated on top of PBE

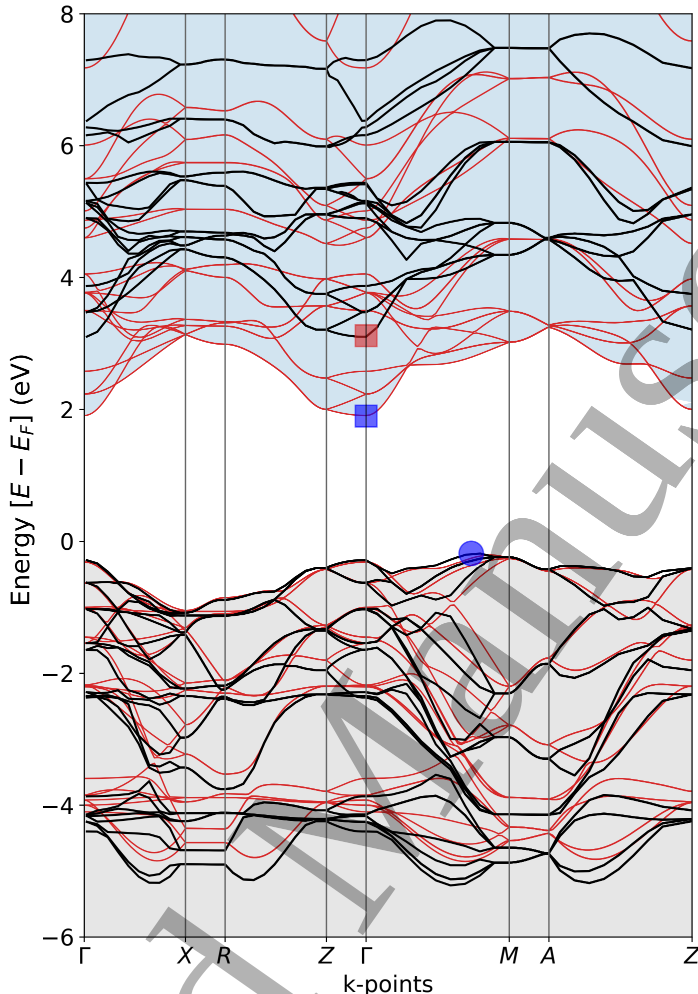

Figure 2. The HSE06(20) and GGA(PBE) band structure calculated along the $\Gamma-X-R-Z-\Gamma-M-A-Z$ high symmetric directions in the irreducible Brillouin zone (IBZ) of anatase TiO_2. The red and black curves represent the PBE and HSE06(20) bands, respectively. The Fermi energy is taken as the reference for energy. The red and blue squares label the conduction band minimum as obtained in HSE06(20) and GGA(PBE) bandstructure, respectively. The blue circle labels the valence band maximum, which is the same with both GGA and HSE06(20).

band gap (G_0W_0@PBE) is 3.8 eV, while the gaps calculated with G_0W_0@HSE06(α) are even larger. As the amount of exact exchange is increased, the quasiparticle gap also increases in proportion: 4.10, 4.17, and 4.25 eV for $\alpha = 20, 25$ and 30 %, respectively. Coming from PBE to HSE06(α), the introduction of exact exchange partially corrects for the self-energy and opens up the bandgap. Compared to PBE, hybrid functionals modify the electronic screening due to the presence of non-local exact exchange, bringing the quasiparticle character of the excitation to prominence. It is also evident from the amount of quasiparticle correction over PBE and HSE06(α) starting points. We obtain a G_0W_0 quasiparticle gap of 3.8 eV over PBE wave starting point with a bandgap of 2.11 eV, leading to a quasiparticle correction of 1.69 eV. At the same time,

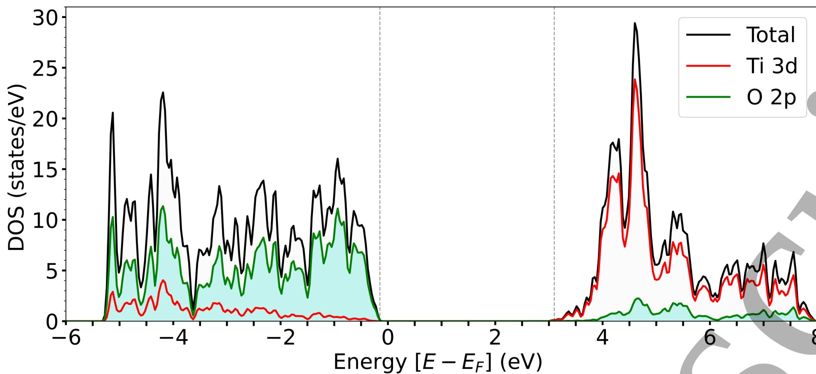

Figure 3. The total and orbital decomposed density of states showing the Ti-3d and O-2p contributions to the local density of states: Energies in DOS are labelled with reference to Fermi energy.

Table 1. G_0W_0 Quasiparticle gap ($E_{QP}^{G_0W_0}$) and BSE optical gaps (E_{Opt}^{BSE}) obtained in the present work, in comparison with literature data determined using different DFT starting points. Available experimentally measured quasiparticle gaps(E_{QP}^{Exp}) and direct optical gaps(E_{Opt}^{Exp}) are also listed for comparison. The symbols I and D in parentheses of quasiparticle gaps denote if the band gaps are indirect or direct, respectively.

	G_0W_0 QP Gap(eV)		BSE Optical gap(eV)		Exp.(eV)	
Starting Point	$E_{QP}^{G_0W_0}$	Ref.	E_{Opt}^{BSE}	Ref.	E_{QP}^{Exp}	E_{Opt}^{Exp}
HSE06(20)	4.10(I)/4.14(D)	This work	3.911	This work	3.97(D)[42]	3.79[42]
HSE06(25)	4.17(I)/4.21(D)	This work	3.455	[72]		3.8 [147]
HSE06(30)	4.25(I)/4.29(D)	This work				3.69[148]
HSE06	3.89(I)	[140]				
HSE06	4.05(I)	[41]				
HSE	4.28(I)	[49]				
	3.8(I)/3.838(D)	This work	3.745	This work		
	3.56(I)/4.14(D)	[40]	3.57	[41]		
	3.83(I)/4.29(D)	[39]	3.90	[39]		
	3.73(I)/3.78(D)	[41]	3.76	[42]		
LDA/GGA	3.73(I)	[95]	4.0	[40, 135]		
	3.7(I)	[149]	4.5	[41]		
	3.791(I)	[36]	3.641	[150]		
	3.46(I)/3.92(D)†	[42]				
	3.92(I)	[60]				
	3.5(I)/3.8(D)	[151]				
	3.866(I)	[150]				
	4.03(I)	[49]				
GGA+U	3.27	[149]				

†3.92 eV(D), the direct gap at Γ point, is obtained after correcting for redshift of 150 meV as a result of zero-point renormalization(ZPR) of the bandgap. In the absence of ZPR the direct gap at Γ point is 4.07 eV.

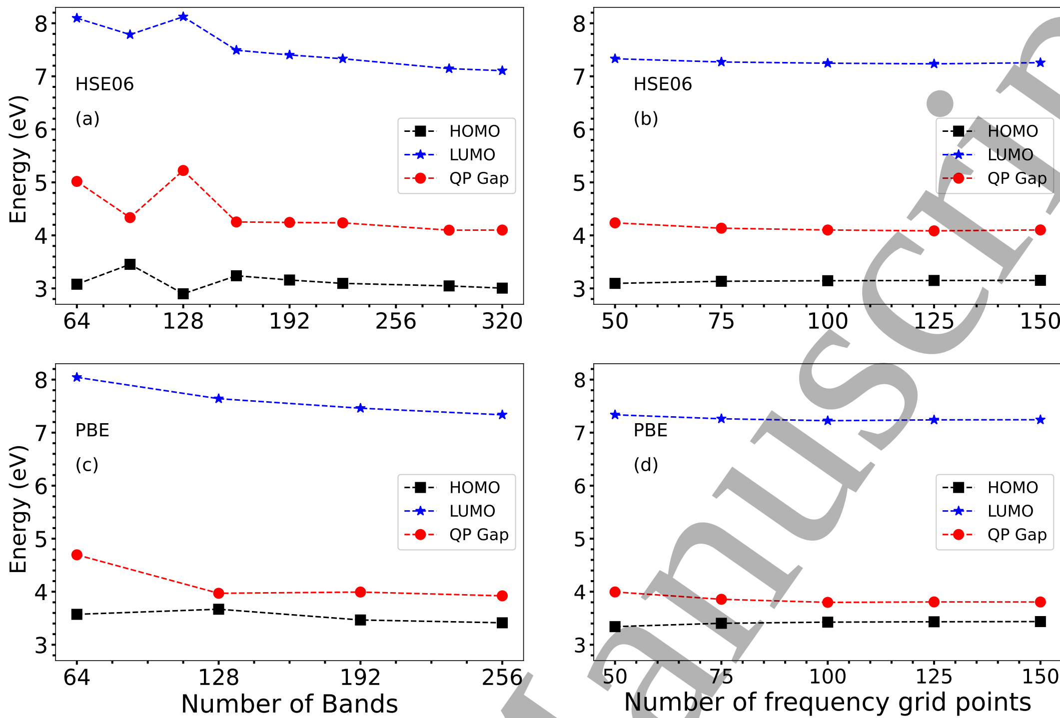

Figure 4. Convergence of G_0W_0 HOMO and LUMO energies, and bandgaps with respect to number of bands and number of frequency grid points for both PBE and HSE06(20) starting wave functions. Convergence is similar for both GGA and HSE06 starting wave functions

HSE06(20) bandgap is 3.34 eV, and the G_0W_0 gap calculated over it is 4.1 eV, implying a correction only by 0.76 eV. With HSE06(25) and HSE06(30) starting points, the respective quasiparticle corrections are 0.49 and 0.24 eV. It indicates that, by tuning α, one can attribute the desired amount of quasiparticle character to the HSE06(α) wave functions.

Unlike KS-DFT band gaps, G_0W_0 quasiparticle gaps can be directly compared with bandgaps measured using angle-resolved photoemission spectroscopy (ARPES). Recently, Ref. [42] reported the direct bandgap of single-crystalline anatase TiO_2 to be 3.97 eV at the Γ point. Compared with this measurement, our G_0W_0@HSE06(20) yields an overestimated value of 4.14 eV. On the other hand, the direct quasiparticle gap at the G_0W_0@PBE level is 3.838 eV. G_0W_0 calculation of anatase TiO_2 starting from LDA/GGA and GGA+U wave functions were explored previously by some studies(Table 1). Quasiparticle gap obtained from these calculations ranges from 3.27 to 4.03 eV. Our G_0W_0@PBE is also within this range. Unlike G_0W_0@PBE calculations, G_0W_0 calculations of anatase TiO_2 starting from hybrid functional DFT have been quite sparse in the literature. Apart from the present work, Ref. [41] and Ref. [140] reported 3.89 eV and 4.05 eV, respectively, with standard HSE06 functional starting points. A much larger value of 4.28 eV was reported in Ref. [49] using HSE functional(unscreened). G_0W_0 on top of standard hybrid functional is seen to overestimate the bandgap compared to experimental values. Nevertheless, as we have shown in the present work, we can improve this by tuning the amount of exact exchange.

Overall, the huge variability of G_0W_0 quasiparticle gaps in Table 1 shows the poor consensus in the literature regarding the calculated quasiparticle bandgap of anatase TiO_2, revealing its strong sensitivity to computational setting and initial structural geometries. The variability can sometimes be attributed to the difference in pseudopotentials used for different calculations. However, it was reported that the variation is not more than 30 meV compared to an all-electron calculation of a given system[49]. An important yet usually ignored origin of discrepancy is the neglect of zero-point renormalization (ZPR) of electronic structure. At low temperatures, ZPR of the bandgap of anatase TiO_2 is a dominant effect causing a redshift of 150 meV for the quasiparticle gap[42]. Including the effect of ZPR, Ref. [42] estimated a quasiparticle gap of 3.92 eV using G_0W_0 with PBE functionals, which is in excellent agreement with their own ARPES data (3.97 eV) mentioned above. In most of the other G_0W_0 calculations in the literature, the effect of ZPR is unaccounted for. In our case, considering the redshift of 150 meV due to the ZPR, direct G_0W_0 gaps calculated using HSE06(20) and PBE functionals are 3.99 eV and 3.68 eV, respectively.

For the quasiparticle gaps to become independent of the starting wavefunctions and eigenvalues, the G and W might be determined self-consistently. However, in the case of anatase TiO_2 this does not lead to an improvement. In Ref. [49] it was found that the quasiparticle gap of anatase TiO_2 increases as the self-consistency level is ratcheted up from G_0W_0, GW_0 and GW, and a 50 % overestimation is noticed with GW calculations. For the self-consistent GW_0 and GW, their quasiparticle gaps are still larger than the G_0W_0@HSEO06(20) presented in our work. Interestingly, Ref. [49] obtained a better agreement of the quasiparticle gap with experiment when the self-consistency is limited only in Green's functions(G), while keeping the screening fixed at the initial non-interacting KS-DFT level (i.e., GW_0 method). However, as shown in this work, adjusting the screening by varying α in the HSE06-like functional, one can obtain a reasonably accurate value of quasiparticle gaps with G_0W_0 itself, with the same accuracy of self-consistent calculations but with a much lesser computational cost.

3.3. Optical transitions

The imaginary part of dielectric function ($\epsilon_2(\omega)$) of pristine anatase TiO_2 obtained from BSE using screened Coulomb interaction(W_0) from G_0W_0@HSE06(α) and G_0W_0@PBE is presented in the Fig.5. Our BSE results from HSE06(α) and PBE starting point will be labelled BSE@HSE06(α) and BSE@PBE, respectively, in spite of the fact that the intermediate G_0W_0 calculation is always performed. Since we are interested only in the low energy excitation spectra, 20 BSE eigenvalues for the incident light polarized parallel and perpendicular to the c-axis are computed in the BSE step. The exciton wavefunctions can be expressed in a coupled electron-hole pair configuration $|S\rangle = \Sigma_{vck} A^S_{vck} |vc\rangle$, where v and c are valence and conduction band states at the k

point, and A^S_{vck} is the eigenvector of the Bethe-Salpeter Equation (Eq. 2) with eigenvalue E^S_{exc}. The eigenstate corresponding to the first bright exciton from the BSE eigenvalue problem of Eq. 2 is visualized in a fatband form[126–129]. It is followed by a discussion on the role of exact exchange in the optical gap, the exciton binding energy and spatial localization of excitons of anatase TiO_2.

The first bright exciton peak in the optical spectra, which defines the optical gap, is converged when 256 bands, $6 \times 6 \times 3$ k-points, 8 topmost valence bands and 16 lowest conduction bands are used while solving the BSE(see supplementary information). For a proper description of screening effects and many-body corrections of TiO_2 even larger number of bands and a much denser k-point sampling would have to be used[42], which is beyond the limits of our computational resources at present. Hence, within the level of convergence possible with this setup, we demonstrate the effect of H-F exchange by obtaining theoretical estimates at affordable level of numerical precision.

In Fig.5, taking the anisotropy associated with the tetragonal symmetry of the anatase TiO_2 lattice into account, we resolve the $\epsilon_2(\omega)$ into two components- $E \perp c$ which is the average over the x and y components and the $E \parallel c$(the z component). At the outset, it is interesting to note that the oscillator strengths of transitions and over all profile of the dielectric function is independent of the DFT starting point used for BSE calculations. This is due to the similarity of band dispersion and density of states irrespective of the choice of PBE and HSE06(α) exchange-correlations. Moreover, the optical gap (first peak of ϵ_2) occurs for the $E \perp c$ component, also irrespective of the starting wave functions. For BSE@PBE as well as BSE@HSE06(α), optical gap lies below the respective direct quasiparticle bandgap, confirming that the first direct optical excitation of anatase TiO_2 is dominated by bound excitons. All other excitations are resonant excitations for BSE@PBE as well as BSE@HSE06(α).

The optical gap and binding energy of first bright exciton in anatase TiO_2 exhibit strong sensitivity to the exchange-correlation functional present in the non-interacting KS Hamiltonian. With PBE starting points, due to the smaller bandgap and overscreening associated with it, the binding energy of excitons for the first peak at 3.745 eV is 93±10 meV. On the other hand, in any case, BSE@HSE06(α) optical gap is larger than that obtained from BSE@PBE. Non-local exact exchange present in the hybrid functional and associated electronic screening shifts the BSE@HSE06(α) peaks towards higher energies than BSE@PBE peaks (Table 2). With HSE06(20) functional starting point, we obtain an optical gap of 3.911 eV, creating excitons which are bound with respect to the direct quasiparticle gap of 4.14 eV. The exciton binding energy corresponding to this excitation, calculated as the difference between the optical gap and the direct quasiparticle G_0W_0 gap, is 229±10 meV. For α = 25 and 30 %, first peak is still present below the direct quasiparticle gap, but are blue shifted compared to BSE@HSE06(20). The exciton binding energy also increases in proportion to α. Optical gap (exciton binding energy) for 25 and 30% are 3.949 eV (261±10 meV) and 3.992 eV (298±10 meV), respectively. With an increase in the amount of H-F exchange (α), the quasiparticle gap (G_0W_0 bandgap) becomes wider (Table 2). A larger electronic

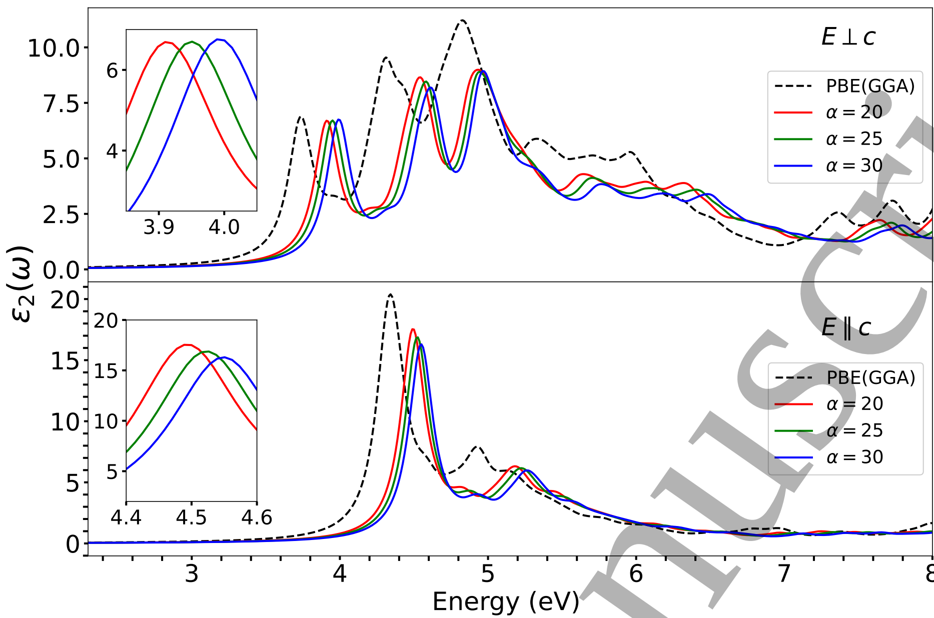

Figure 5. Variation in the imaginary part of dielectric function of anatase TiO_2 for in-plane and perpendicular polarization as a function of the fraction of H-F exchange(α) in the modified(HSE06) starting point for BSE calculation. The peak correspond to first direct optical transition is blue-shifted as the value of α is increased. Similarly, the excitons become more strongly bound as α is increased (see Table 2).

gap makes the electronic screening less efficient, and consequently the electron-hole interaction is less screened. Therefore, the electron-hole pairs in the interacting levels becomes more strongly bound as the amount of exact exchange is increased.

In the fatband representation shown in Fig.6, the black and green open squares are Kohn-Sham eigenvalues in the valence band and conduction band, respectively. At a given k -point, pairs of circles of identical color and radii present in the valence band and the conduction band represent quasiparticle electron-hole pair forming the exciton. The size of the circle denotes the absolute value of the amplitude $\mid A^S_{vc} \mid$ as used in the Eq. 2. It is apparent from the Fig. 6 that only two highest occupied bands ($v = 7, 8$) and two lowest unoccupied bands ($c = 9, 10$) considered for BSE are involved for the first bright transition (optical gap). The most important part of the Brillouin zone responsible for the BSE@HSE06(20) excitonic peak at 3.911 eV lies along the $\Gamma - Z$ directions. Within the resolution of k-space available in our BSE calculation, we can assert that other regions contribute only weakly. This observation holds true irrespective of PBE or HSE06(α) exchange-correlation used, and independent of amount of exact exchange (supplementary information).

Combining Fig.6 with the orbital projected HSE06(20) and PBE density of states in the supplementary information, we identify that O-p_x, p_y states make up most of the $v = 7, 8$ bands and Ti-d_{xy} states occupy the $c = 9, 10$ bands. Dispersion of the lowest conduction band and the highest valence band in the $\Gamma - Z$ direction are nearly parallel, leading to similar electron and hole group velocities in this region. This provides a large

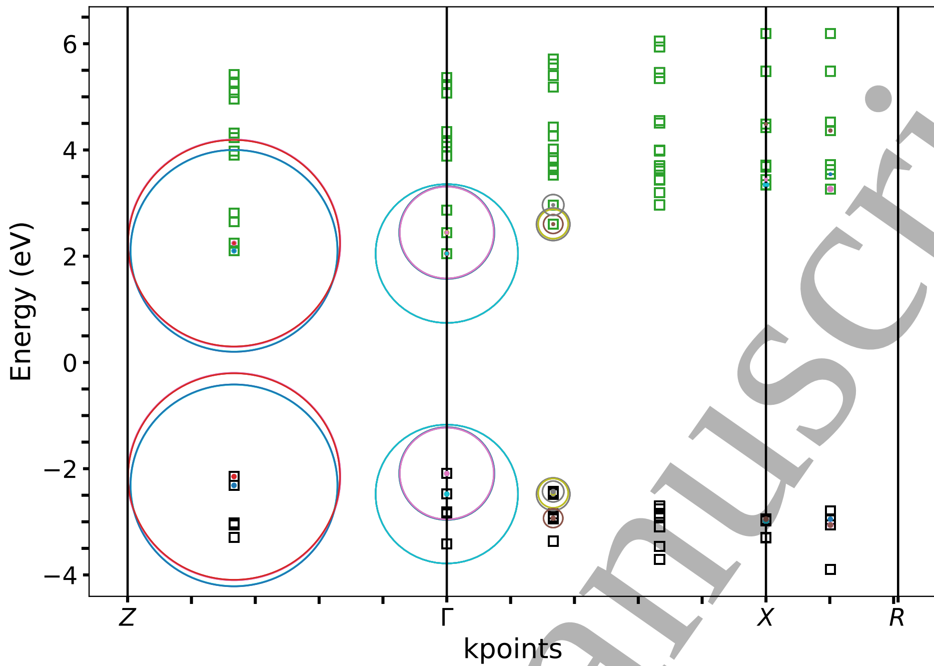

Figure 6. Eigenstates of the first bright transition of anatase TiO_2 is visualized along with the relative coupling strength of quasiparticle electron-hole pair in fatband style. Black and green open squares in the fatband are Kohn-Sham eigenvalues in the valence band and conduction band, respectively. Energies in the plot are shifted to make Fermi energy zero. The pairs of circles of same color and radii, one centered at a hole eigenvalue from the valence band and the other at an electron eigenvalue at the conduction band at a given k-vector represent an electron-hole pair. The radius of the circle is an indicative of relative coupling strength of individual exciton. The Γ and Z region of the Brillouin zone predominantly contribute to the first excitonic transitions while the rest of the regions contributes only weakly. This clearly shows the localization of excitons in the plane perpendicular to the c-axis of anatase unit cell.

joint density of states for the optical transitions providing stability and strong binding of excitons. Flatness of topmost valence band and bottom most conduction bands in the $\Gamma - Z$ direction indicates that orbital interactions in anatase TiO_2 mainly run in the xy plane than in the z direction in the real space[152]. As excitonic states are also from the same region of the Brillouin zone, this immediately translate into localization of excitons on the xy plane in real space. Similar observation has been made by Ref. [153] and Ref. [42] wherein it is shown that high degree of localization of bound exciton confine the excitons almost in a single atomic plane(in the xy plane). Besides, the localization of excitons predicted in this work with BSE-G_0W_0-HSE06(20) agrees well with the analysis of spatial distribution of the exciton wave functions in real space by Ref. [39] and Ref. [154].

While comparing the present BSE calculation with the experiments it must be considered that the present BSE calculations include only coupling of direct electron-hole transitions. Hence, possible interactions originating from the indirect nature of the material would not be considered. The excitons described in our BSE calculation are

Table 2. HSE06(α) indirect gap ($E^I_{HSEO6}(\alpha)$), Indirect and direct quasiparticle gap (E^I_{QP}, E^D_{QP}), quasiparticle correction over indirect bandgap ($E^I_{QP} - E^I_{HSEO6}(\alpha)$), BSE optical gaps ($E^D_{Optical}$) and exciton binding energy of anatase TiO_2 as a function of H-F exchange fraction(α) in the HSE06(α) set-up.

α (%)	$E^I_{HSEO6}(\alpha)$ (eV)	E^I_{QP} (eV)	$E^I_{QP} - E^I_{HSEO6}(\alpha)$ (eV)	E^D_{QP} (eV)	$E^D_{Optical}$ (eV)	EB (meV)
PBE	2.11	3.80	1.69	3.838	3.745	93
20	3.34	4.10	0.76	4.14	3.911	229
25	3.68	4.17	0.49	4.21	3.949	261
30	4.01	4.25	0.24	4.29	3.992	298

screened by the electronic component alone. Ionic relaxation and lattice rearrangements accompanying exciton formation[155] and the influence of intrinsic defects[143, 156] are not taken into account in our calculation. Experiments would generally involve the effects of temperatures and indirect processes like the electron-phonon interactions. In the case of pristine anatase TiO_2, as evidenced by the large difference between static and optical dielectric constants (static (optical) dielectric constants : 45.1(5.82) for $E \perp c$ and 22.7(5.41) for $E \parallel c$), the lattice relaxation has strong influence on the dynamics of excited charges[157]. Moreover, at finite temperatures, electron-phonon interactions and lattice thermal expansion affect temperature band gap renormalization in anatase TiO_2[20]. In several experimental investigations, the absorption edge of anatase TiO_2 was reported to be in the range 3.2-3.8 eV from optical measurements[147, 158–160]. These measurements are affected by indirect processes described above[21, 135, 158, 161–165].

Since our BSE optical gap can only be compared with measured direct optical gaps we look at the reported values of transitions of anatase TiO_2 that have been previously found by spectroscopic ellipsometry at 3.8 eV, and 3.79 eV, respectively, by Ref. [147] and Ref. [42] and at 3.69 eV by photoluminescence as in Ref. [148]. Our estimate of BSE direct optical gap of 3.911 eV computed over HSE06(20) starting wave functions is in close agreement with these experimental data. The deviation from experiment is within a range of ± 0.3 eV, which is quite reasonable, considering the fact that experimental errors and temperature effects need to be accounted for as well.

Theoretical estimate of optical gaps by BSE calculations of pristine anatase TiO_2 lies in a wide range from 3.45 to 4.5 eV (Table 1). In the literature, however, the use of hybrid functional as the starting wave functions for BSE calculation of anatase TiO_2 is not very well explored. One such BSE study reported an optical gap of 3.45 eV[72] for $E \perp c$ polarization using the standard HSE06 functional as starting wave functions. This is the lowest of all available BSE calculations of pristine anatase TiO_2, and is underestimated compared to results obtained using hybrid functionals in present investigation. With PBE functional starting wave function, direct optical gap obtained from BSE calculation for anatase single crystals by Ref. [42](3.76 eV) yields excellent agreement with spectroscopic ellipsometric study (3.79 eV), making it the most reliable estimate of the optical gap so far. In the present work, BSE@PBE and BSE@HSE06(20) yields optical gaps of 3.745 and 3.911 eV, respectively, both of which are very close to experimental values presented in Ref. [42]. However, with regard to exciton binding energy, 160 meV is reported in Ref. [42] from the BSE calculation on PBE starting point. This value has also been verified at low temperatures and measured 180 meV as the binding energy of excitons of anatase TiO_2[42]. In the present work, the exciton binding energy calculated using BSE@HSE06(20), i.e., 229 meV, is closer to this measured value compared to 93 meV estimated with PBE starting point.

Similar to the quasiparticle gap, exciton binding energy also varies linearly in proportion to the amount of exact exchange. A simple linear extrapolation of the available data to the case of zero exact exchange gives 90 meV as the exciton binding energy. This is consistent with the exciton binding energy obtained from pure semi-local(PBE) functional starting point(93 meV). For $\alpha = 20\%$, the relation $\alpha = 1/\epsilon_\infty$ provides an estimate for dielectric constant(ϵ_∞) of 5. This is lower than the experimental dielectric constant of TiO_2 of 5.82 [166]. $\epsilon_\infty = 5.82$ leaves us with a reasonable choice of α of 17.2 %. Extrapolation of BSE@HSE06(α) exciton binding energy to $\alpha = 17.2\%$ yield 208 meV, bringing it further closer to the measured exciton binding energy of 180 meV as in Ref. [42]. However, an exact match of BSE@HSE06(α) exciton binding energy with 180 meV is possible with 13 % of exact exchange.

4. Concluding remarks

In conclusion, we have systematically investigated the effects of the non-interacting KS Hamiltonian on the G_0W_0 quasiparticle gap and the BSE optical spectra of anatase TiO_2. G_0W_0 and BSE calculations are carried out starting from HSE06 type functionals, which mixes 20, 25 and 30 % exact Hartree-Fock exchange and with GGA(PBE) functional. We have shown that the values of quasiparticle gap, optical gap and exciton binding energies exhibit strong sensitivity to the starting DFT wave functions. The starting point dependence is mainly introduced through the dielectric screening evaluated at the G_0W_0 step. However, except for the bandgap variation, the electronic bandstructure and the density of states are very similar irrespective of the functionals employed. Furthermore, the qualitative features of the optical dielectric function, i.e., the shape and oscillator strengths and spatial localization of excitons, are also insensitive to the choice of exchange-correlation functional.

G_0W_0 quasiparticle gap of anatase TiO_2 computed over hybrid functional starting points is typically overestimated compared to measured values. However, by tuning the amount of exact exchange, the dielectric screening can be varied, hence the quasiparticle gap. Due to the non-local exact exchange contribution, the W_0 constructed from HSE06(α) would be expected to lead to lesser screening than that constructed from PBE functional. Therefore, G_0W_0 gaps of anatase TiO_2 on HSE06(α) starting points tend to be larger than G_0W_0@PBE gaps. Similar to G_0W_0 gaps, the exciton binding energy also increases in proportion to the amount of exact exchange. A simple extrapolation of the calculated data leads to the result so that, with 13 % of exact exchange, we can obtain an exact match with the recently measured value.

References

[1] Fujishima A and Honda K 1972 *nature* **238** 37–38

[2] Fujishima A, Rao T N and Tryk D A 2000 *Journal of photochemistry and photobiology C: Photochemistry reviews* **1** 1–21

[3] Mills A, Elliott N, Hill G, Fallis D, Durrant J R and Willis R L 2003 *Photochemical & Photobiological Sciences* **2** 591–596

[4] Bai Y, Mora-Sero I, De Angelis F, Bisquert J and Wang P 2014 *Chemical reviews* **114** 10095–10130

[5] Chen S, Yu M, Han W P, Yan X, Liu Y C, Zhang J C, Zhang H D, Yu G F and Long Y Z 2014 *RSC advances* **4** 46152–46156

[6] Grätzel M 2005 *Inorganic chemistry* **44** 6841–6851

[7] O'regan B and Gratzel M 1991 *nature* **353** 737–740

[8] Hagfeldt A and Grätzel M 2000 *Accounts of Chemical Research* **33** 269–277

[9] Agrawal S, English N J, Thampi K R and MacElroy J 2012 *Physical Chemistry Chemical Physics* **14** 12044–12056

[10] Thompson T L and Yates J T 2006 *Chemical reviews* **106** 4428–4453

[11] Chen X and Mao S S 2007 *Chemical reviews* **107** 2891–2959

[12] Khan S U, Al-Shahry M and Ingler W B 2002 *science* **297** 2243–2245

[13] Varghese O K, Paulose M, LaTempa T J and Grimes C A 2009 *Nano letters* **9** 731–737

[14] Alotaibi A M, Williamson B A, Sathasivam S, Kafizas A, Alqahtani M, Sotelo-Vazquez C, Buckeridge J, Wu J, Nair S P, Scanlon D O *et al.* 2020 *ACS applied materials & interfaces* **12** 15348–15361

[15] Yaqub N, Farooq W and AlSalhi M 2021 *Journal of King Saud University-Science* 101723

[16] Xu M, Gao Y, Moreno E M, Kunst M, Muhler M, Wang Y, Idriss H and Woll C 2011 *Physical Review Letters* **106** 138302

[17] Carp O, Huisman C L and Reller A 2004 *Progress in solid state chemistry* **32** 33–177

[18] Luttrell T, Halpegamage S, Tao J, Kramer A, Sutter E and Batzill M 2014 *Scientific reports* **4** 1–8

[19] Sumita T, Yamaki T, Yamamoto S and Miyashita A 2002 *Applied Surface Science* **200** 21–26

[20] Wu Y N, Wuenschell J K, Fryer R, Saidi W A, Ohodnicki P, Chorpening B and Duan Y 2020 *Journal of Physics: Condensed Matter* **32** 405705

[21] Tang H, Prasad K, Sanjines R, Schmid P and Levy F 1994 *Journal of applied physics* **75** 2042–2047

[22] Tamaki Y, Furube A, Murai M, Hara K, Katoh R and Tachiya M 2007 *Physical Chemistry Chemical Physics* **9** 1453–1460

[23] Yamamoto S, Sumita T, Miyashita A *et al.* 2001 *Journal of Physics: Condensed Matter* **13** 2875

[24] Ding Y, Ding B, Kanda H, Usiobo O J, Gallet T, Yang Z, Liu Y, Huang H, Sheng J, Liu C *et al.* 2022 *Nature Nanotechnology* 1–8

[25] Kang X, Liu S, Dai Z, He Y, Song X and Tan Z 2019 *Catalysts* **9** 191

[26] Pelaez M, Nolan N T, Pillai S C, Seery M K, Falaras P, Kontos A G, Dunlop P S, Hamilton J W, Byrne J A, O'shea K *et al.* 2012 *Applied Catalysis B: Environmental* **125** 331–349

[27] Peng H, Li J, Li S S and Xia J B 2008 *Journal of Physics: Condensed Matter* **20** 125207

[28] Atambo M O, Varsano D, Ferretti A, Ataei S S, Caldas M J, Molinari E and Selloni A 2019 *Physical Review Materials* **3** 045401

[29] Ma Z, Ren F, Yang Z and Volinsky A A 2021 *Optik* **241** 167107

[30] Li C, Zhao Y, Gong Y, Wang T and Sun C 2014 *Physical Chemistry Chemical Physics* **16** 21446–21451

[31] Meng Q, Wang T, Liu E, Ma X, Ge Q and Gong J 2013 *Physical Chemistry Chemical Physics* **15** 9549–9561

[32] Liu J, Weng M, Li S, Chen X, Cen J, Jie J, Xiao W, Zheng J and Pan F 2020 *Physical Chemistry Chemical Physics* **22** 39–53

[33] Jensen S and Kilin D S 2015 *Journal of Physics: Condensed Matter* **27** 134207

[34] Ghuman K K and Singh C V 2013 *Journal of Physics: Condensed Matter* **25** 475501

[35] Bettinelli M, Speghini A, Falcomer D, Daldosso M, Dallacasa V and Romanò L 2006 *Journal of Physics: Condensed Matter* **18** S2149

[36] Thulin L and Guerra J 2008 *Physical Review B* **77** 195112

[37] Wang Z, Saxena S, Pischedda V, Liermann H and Zha C 2001 *Journal of Physics: Condensed Matter* **13** 8317

[38] Thilagam A, Simpson D and Gerson A 2010 *Journal of Physics: Condensed Matter* **23** 025901

[39] Chiodo L, García-Lastra J M, Iacomino A, Ossicini S, Zhao J, Petek H and Rubio A 2010 *Physical Review B* **82** 045207

[40] Kang W and Hybertsen M S 2010 *Physical Review B* **82** 085203

[41] Landmann M, Rauls E and Schmidt W 2012 *Journal of physics: condensed matter* **24** 195503

[42] Baldini E, Chiodo L, Dominguez A, Palummo M, Moser S, Yazdi-Rizi M, Auböck G, Mallett B P, Berger H, Magrez A *et al.* 2017 *Nature communications* **8** 1–11

[43] Tosoni S, Di Liberto G and Pacchioni G 2020 *Titanium Dioxide (TiO2) and Its Applications* 67

[44] Jin F, Zhang X, Wei M, Chen T, Ma H and Ma Y 2020 *Journal of Materials Chemistry A* **8** 20082–20090

[45] Aulbur W G, Jönsson L and Wilkins J W 2000 *Solid state physics (New York. 1955)* **54** 1–218

[46] Hybertsen M S and Louie S G 1986 *Physical Review B* **34** 5390

[47] Nguyen H V, Pham T A, Rocca D and Galli G 2012 *Physical Review B* **85** 081101

[48] Salpeter E E and Bethe H A 1951 *Physical Review* **84** 1232

[49] Kang G, Kang Y and Han S 2015 *Physical Review B* **91** 155141

[50] Caruso F, Rinke P, Ren X, Scheffler M and Rubio A 2012 *Physical Review B* **86** 081102

[51] Shishkin M and Kresse G 2007 *Physical Review B* **75** 235102

[52] Kotani T, van Schilfgaarde M and Faleev S V 2007 *Physical Review B* **76** 165106

[53] van Schilfgaarde M, Kotani T and Faleev S 2006 *Physical review letters* **96** 226402

[54] Holm B and von Barth U 1998 *Physical Review B* **57** 2108

[55] Gerosa M, Bottani C, Di Valentin C, Onida G and Pacchioni G 2017 *Journal of Physics: Condensed Matter* **30** 044003

[56] Morales-García Á, Valero R and Illas F 2017 *Journal of chemical theory and computation* **13** 3746–3753

[57] Hybertsen M S and Louie S G 1985 *Physical review letters* **55** 1418

[58] Bechstedt F, Del Sole R, Cappellini G and Reining L 1992 *Solid state communications* **84** 765–770

[59] Zhu T and Gao S P 2014 *The Journal of Physical Chemistry C* **118** 11385–11396

[60] Thatribud A 2019 *Materials Research Express* **6** 095021

[61] Heyd J, Scuseria G E and Ernzerhof M 2003 *The Journal of chemical physics* **118** 8207–8215

[62] Heyd J and Scuseria G E 2004 *The Journal of chemical physics* **120** 7274–7280

[63] Krukau A V, Vydrov O A, Izmaylov A F and Scuseria G E 2006 *The Journal of chemical physics* **125** 224106

[64] Ge H J S and Ernzerhof M 2006 *J Chem Phys* **124** 219906

[65] Bechstedt F, Fuchs F and Kresse G 2009 *physica status solidi (b)* **246** 1877–1892

[66] Schleife A, Varley J, Fuchs F, Rodl C, Bechstedt F, Rinke P, Janotti A and Van de Walle C 2011 *Physical Review B* **83** 035116

[67] Rodl C, Fuchs F, Furthmuller J and Bechstedt F 2009 *Physical Review B* **79** 235114

[68] Fuchs F and Bechstedt F 2008 *Physical Review B* **77** 155107
[69] Fuchs F, Furthmüller J, Bechstedt F, Shishkin M and Kresse G 2007 *Physical Review B* **76** 115109
[70] Cappellini G, Furthmuller J, Cadelano E and Bechstedt F 2013 *Physical Review B* **87** 075203
[71] Isseroff L Y and Carter E A 2012 *Physical Review B* **85** 235142
[72] Basera P, Saini S and Bhattacharya S 2019 *Journal of Materials Chemistry C* **7** 14284–14293
[73] Sham L and Schlüter M 1985 *Physical Review B* **32** 3883
[74] Perdew J P and Zunger A 1981 *Physical Review B* **23** 5048
[75] Perdew J P, Parr R G, Levy M and Balduz Jr J L 1982 *Physical Review Letters* **49** 1691
[76] Perdew J P, Yang W, Burke K, Yang Z, Gross E K, Scheffler M, Scuseria G E, Henderson T M, Zhang I Y, Ruzsinszky A *et al.* 2017 *Proceedings of the National Academy of Sciences* **114** 2801–2806
[77] Perdew J P and Levy M 1983 *Physical Review Letters* **51** 1884
[78] Norman M R and Perdew J P 1983 *Physical Review B* **28** 2135
[79] Cohen A J, Mori-Sánchez P and Yang W 2008 *Physical Review B* **77** 115123
[80] Chan M and Ceder G 2010 *Physical review letters* **105** 196403
[81] Friedrich C, Betzinger M, Schlipf M, Blügel S and Schindlmayr A 2012 *Journal of Physics: Condensed Matter* **24** 293201
[82] Furthmüller J, Hahn P, Fuchs F and Bechstedt F 2005 *Physical Review B* **72** 205106
[83] Deak P 2018 *Physica B: Condensed Matter* **535** 35–43
[84] Yamamoto T and Ohno T 2012 *Physical Chemistry Chemical Physics* **14** 589–598
[85] Anisimov V I, Aryasetiawan F and Lichtenstein A 1997 *Journal of Physics: Condensed Matter* **9** 767
[86] Gillen R and Robertson J 2013 *Journal of Physics: Condensed Matter* **25** 165502
[87] Raghav A, Hanindriyo A T, Utimula K, Abbasnejad M, Maezono R and Panda E 2020 *Computational Materials Science* **184** 109925
[88] Celik V and Mete E 2013 *Journal of Physics: Condensed Matter* **25** 365502
[89] Heyd J, Scuseria G E and Ernzerhof M 2003 *The Journal of Chemical Physics* **118** 8207–8215
[90] Paier J, Marsman M, Hummer K, Kresse G, Gerber I C and Ángyán J G 2006 *The Journal of chemical physics* **124** 154709
[91] Alkauskas A, Broqvist P, Devynck F and Pasquarello A 2008 *Physical review letters* **101** 106802
[92] Alkauskas A, Broqvist P and Pasquarello A 2011 *physica status solidi (b)* **248** 775–789
[93] Alkauskas A, Broqvist P and Pasquarello A 2008 *Physical review letters* **101** 046405
[94] de PR Moreira I, Illas F and Martin R L 2002 *Physical Review B* **65** 155102
[95] Gerosa M, Bottani C E, Caramella L, Onida G, Di Valentin C and Pacchioni G 2015 *Physical Review B* **91** 155201
[96] Marques M A, Vidal J, Oliveira M J, Reining L and Botti S 2011 *Physical Review B* **83** 035119
[97] Skone J H, Govoni M and Galli G 2014 *Physical Review B* **89** 195112
[98] Garza A J and Scuseria G E 2016 *The journal of physical chemistry letters* **7** 4165–4170
[99] Kresse G and Hafner J 1993 *Physical Review B* **48** 13115
[100] Hafner J 2008 *Journal of computational chemistry* **29** 2044–2078
[101] Kresse G and Furthmüller J 1996 *Physical review B* **54** 11169
[102] Kresse G and Furthmüller J 1996 *Computational materials science* **6** 15–50
[103] Shishkin M and Kresse G 2006 *Physical Review B* **74** 035101
[104] Blöchl P E 1994 *Physical review B* **50** 17953
[105] Kresse G and Joubert D 1999 *Physical review b* **59** 1758
[106] Monkhorst H J and Pack J D 1976 *Physical review B* **13** 5188
[107] Burdett J K, Hughbanks T, Miller G J, Richardson Jr J W and Smith J V 1987 *Journal of the American Chemical Society* **109** 3639–3646
[108] Rao K K, Naidu S N and Iyengar L 1970 *Journal of the American Ceramic Society* **53** 124–126
[109] Howard C, Sabine T and Dickson F 1991 *Acta Crystallographica Section B: Structural Science*

47 462–468
[110] Janesko B G, Henderson T M and Scuseria G E 2009 *Physical Chemistry Chemical Physics* **11** 443–454
[111] Viñes F, Lamiel-García O, Chul Ko K, Yong Lee J and Illas F 2017 *Journal of computational chemistry* **38** 781–789
[112] He J and Franchini C 2012 *Physical Review B* **86** 235117
[113] Koller D, Blaha P and Tran F 2013 *Journal of Physics: Condensed Matter* **25** 435503
[114] Ko K C, Lamiel-García O, Lee J Y and Illas F 2016 *Physical Chemistry Chemical Physics* **18** 12357–12367
[115] Zhang Y f, Lin W, Li Y, Ding K n and Li J q 2005 *The Journal of Physical Chemistry B* **109** 19270–19277
[116] Hedin L 1965 *Physical Review* **139** A796
[117] Aryasetiawan F and Gunnarsson O 1998 *Reports on Progress in Physics* **61** 237
[118] Gerosa M, Bottani C E, Caramella L, Onida G, Di Valentin C and Pacchioni G 2015 *The Journal of chemical physics* **143** 134702
[119] Onida G, Reining L and Rubio A 2002 *Reviews of Modern Physics* **74** 601
[120] Hanke W and Sham L J 1979 *Phys. Rev. Lett.* **43**(5) 387–390
[121] Sander T, Maggio E and Kresse G 2015 *Physical Review B* **92** 045209
[122] Leng X, Jin F, Wei M and Ma Y 2016 *Wiley Interdisciplinary Reviews: Computational Molecular Science* **6** 532–550
[123] Dancoff S 1950 *Physical Review* **78** 382
[124] Tamm I 1991 Relativistic interaction of elementary particles *Selected Papers* (Springer) pp 157–174
[125] Shishkin M, Marsman M and Kresse G 2007 *Physical review letters* **99** 246403
[126] Wang X, Meng W and Yan Y 2017 *Journal of Applied Physics* **122** 085104
[127] Bokdam M, Sander T, Stroppa A, Picozzi S, Sarma D, Franchini C and Kresse G 2016 *Scientific reports* **6** 1–8
[128] Kolos M and Karlickỳ F 2019 *Physical Chemistry Chemical Physics* **21** 3999–4005
[129] Cocchi C, Moldt T, Gahl C, Weinelt M and Draxl C 2016 *The Journal of Chemical Physics* **145** 234701
[130] Çelik V and Mete E 2012 *Physical Review B* **86** 205112
[131] Mo S D and Ching W 1995 *Physical Review B* **51** 13023
[132] Boonchun A, Reunchan P and Umezawa N 2016 *Physical Chemistry Chemical Physics* **18** 30040–30046
[133] Asahi R, Taga Y, Mannstadt W and Freeman A J 2000 *Physical Review B* **61** 7459
[134] Lucovsky G 2001 *Journal of Optoelectronics and Advanced Materials* **3** 155–166
[135] Lawler H, Rehr J, Vila F, Dalosto S D, Shirley E L and Levine Z H 2008 *Physical Review B* **78** 205108
[136] Fischer D W 1972 *Physical Review B* **5** 4219
[137] Modrow H, Bucher S, Rehr J and Ankudinov A 2003 *Physical Review B* **67** 035123
[138] Tang W, Sanville E and Henkelman G 2009 *Journal of Physics: Condensed Matter* **21** 084204
[139] Deak P, Aradi B and Frauenheim T 2012 *Physical Review B* **86** 195206
[140] Dou M and Persson C 2013 *Journal of Applied Physics* **113** 083703
[141] Deak P, Aradi B and Frauenheim T 2011 *Physical Review B* **83** 155207
[142] Arroyo-de Dompablo M, Morales-Garcia A and Taravillo M 2011 *The Journal of chemical physics* **135** 054503
[143] Mattioli G, Alippi P, Filippone F, Caminiti R and Amore Bonapasta A 2010 *The Journal of Physical Chemistry C* **114** 21694–21704
[144] Borlido P, Aull T, Huran A W, Tran F, Marques M A and Botti S 2019 *Journal of chemical theory and computation* **15** 5069–5079
[145] Janotti A, Varley J, Rinke P, Umezawa N, Kresse G and Van de Walle C G 2010 *Physical Review*

B **81** 085212
[146] Shih B C, Xue Y, Zhang P, Cohen M L and Louie S G 2010 *Physical review letters* **105** 146401
[147] Wang Z, Helmersson U and Kall P O 2002 *Thin Solid Films* **405** 50–54
[148] Liu B, Wen L and Zhao X 2007 *Materials Chemistry and Physics* **106** 350–353
[149] Patrick C E and Giustino F 2012 *Journal of Physics: Condensed Matter* **24** 202201
[150] Hu L, Xu C, Peng L, Gu F L and Yang W 2018 *Journal of Materials Chemistry A* **6** 15027–15032
[151] Giorgi G, Palummo M, Chiodo L and Yamashita K 2011 *Physical Review B* **84** 073404
[152] Laskowski R, Christensen N E, Blaha P and Palanivel B 2009 *Physical Review B* **79** 165209
[153] Chen H, Dawson J A and Umezawa N 2015 *Physical Review Applied* **4** 014007
[154] Ataei S S, Mohammadizadeh M R and Seriani N 2017 *Physical Review B* **95** 155205
[155] Gallart M, Cottineau T, Hönerlage B, Keller V, Keller N and Gilliot P 2018 *Journal of Applied Physics* **124** 133104
[156] Pascual J, Camassel J and Mathieu H 1978 *Physical Review B* **18** 5606
[157] Gonzalez R, Zallen R and Berger H 1997 *Physical Review B* **55** 7014
[158] Tang H, Levy F, Berger H and Schmid P 1995 *Physical Review B* **52** 7771
[159] Hosaka N, Sekiya T, Fujisawa M, Satoko C and Kurita S 1996 *Journal of electron spectroscopy and related phenomena* **78** 75–78
[160] Hosaka N, Sekiya T and Kurita S 1997 *Journal of luminescence* **72** 874–875
[161] Tang H, Berger H, Schmid P, Levy F and Burri G 1993 *Solid State Communications* **87** 847–850
[162] Persson C and Ferreira da Silva A 2005 *Applied Physics Letters* **86** 231912
[163] Morgan B J and Watson G W 2009 *Physical Review B* **80** 233102
[164] Deskins N A and Dupuis M 2007 *Physical Review B* **75** 195212
[165] Watanabe M and Hayashi T 2005 *Journal of luminescence* **112** 88–91
[166] Wemple S 1977 *The Journal of Chemical Physics* **67** 2151–2168